Journal of Molecular Graphics and Modelling 29 (2010) 581–590

Contents lists available at ScienceDirect

Journal of Molecular Graphics and Modelling

journal homepage: www.elsevier.com/locate/JMGM

Conformational profile of bombesin assessed using different computational protocols

Parul Sharma [a], Parvesh Singh [a], Krishna Bisetty [a], Francesc J. Corcho [b], Juan. J. Perez [b,*]

[a] Department of Chemistry, Durban University of Technology, Steve Biko Campus, P.O. Box 1334, Durban 4000, South Africa
[b] Department d' Enginyeria Quimica, UPC, ETS d'Enginyers Industrials, Av. Diagonal, 647, 08028 Barcelona, Spain

ARTICLE INFO

Article history:
Received 17 August 2010
Received in revised form 28 October 2010
Accepted 9 November 2010
Available online 17 November 2010

Keywords:
Bombesin
Replica exchange
Molecular dynamics
Conformation
Peptide
Computational study

ABSTRACT

The present work involves the study of the conformational profile of bombesin using different computational procedures used to explore the configurational space based on molecular dynamics simulations. Specifically, the present study describes the effect of using Berendsen's versus Langevin's thermostat and on the other hand, the use of the multicanonical replica exchange molecular dynamics as compared to standard molecular dynamics. In these simulations the solvent was modeled using the Onufriev, Bashford and Case implementation of Generalized Born procedure. The detailed computational analysis agrees well with the aggregated information previously reported in the NMR study of the peptide in a mixture of trifluoroethanol/water. Present results show a clear preference for the peptide to attain a helical structure on the segment 6–14, with a tendency to adopt a α-helix at the C-terminus aligning the aromatic residues Trp^{8} and His^{12} together with Gln^{7}, known to be important for peptide mediated activation. Finally, the three methodologies used in the present work yield similar structural results, although a detailed analysis reveals biases that need to be considered when performing this kind of studies.

1. Introduction

Besides the so-called mini-proteins, in solution the vast majority of short polypeptide chains exhibit a complex conformational profile as a result of a dynamical exchange between conformations at the microscopic level, due to its flexible nature [1]. This behavior is solvent dependent so that, in solvents with a high hydrogen bond formation capability and low viscosity like water, peptides normally exhibit random coil profiles whereas in structuring solvents, specific structural features can often be identified [2]. Accordingly, it is expected that experimental techniques reveal average features of the structure as the result of the superimposition of diverse coexisting structures of the ensemble. The conformational features of the polypeptide are dictated by complex balance of molecular interactions determined by the amino acid sequence and modulated by the environment. In geometrical terms this leads to a rugged potential energy surface with multiple minima, whose characterization through atomistic simulations represent a complementary *bottom–up* approach to understand the conformational features of a peptide in solution.

The exploration of the conformational space of a peptide is a topic widely discussed in the literature [3]. Sampling can be carried out either through a topographical exploration of the potential energy surface using methods like simulated annealing (SA) [4], or in the configurational space using methods like Monte Carlo (MC) or molecular dynamics (MD) [5]. However, due to the nature of the conformational energy surface, sampling engines can be trapped in local minima, being a fundamental task to assess the extent of the space already sampled. For methods that explore the potential energy surface, a qualitative knowledge of the extent of the space sampled can be assessed by inspection of the density of states characterized during the sampling process [6]. In contrast, sampling the configurational space convergence is achieved when a Maxwell–Boltzmann weighted ensemble is obtained [7].

The present work is intended to get some insight into the performance of different procedures used to explore the configurational space based on molecular dynamics simulations to provide an adequate atomic description of the system, compatible with the aggregated information provided by different experimental techniques. Specifically, in the present work we report the results of the exploration of the conformational space of a medium size peptide using standard molecular dynamics calculations at 300 K using two different thermostats: first, Berendsen's thermostat [8] and second, Langevin's thermostat [9]. The former is widely used in biomolecular simulations because of its stability and efficiency, although in contrast to the latter, it does not produce canonical distributions. In addition, we want also to compare the results obtained from a molecular dynamics trajectory with those produced using the multicanonical replica exchange molecular dynamics method for sampling purposes using the same thermostat [10].

* Corresponding author.
E-mail address: juan.jesus.perez@upc.edu (Juan.J. Perez).

1093-3263/$ – see front matter © 2010 Elsevier Inc. All rights reserved.
doi:10.1016/j.jmgm.2010.11.006

We considered for the present study the tetradecapeptide of sequence: Glp-Gln-Arg-Leu-Gly-Asn-Gln-Trp-Ala-Val-Gly-His-Leu-Met-NH2 (Glp = pyroglutamic acid) known as bombesin, due to its pharmacological relevance. Originally isolated from the frog skin of the amphibian *Bombina bombina* [11], it belongs to a family of compounds that exhibit a variety of biological activities in numerous tissues and cell types [12] and it is widely distributed in different regions of brain, lung and gastrointestinal tracts [13,14]. Bombesin acts as a neurotransmitter and a neuromodulator on the peripheral system by stimulating the muscles of the alimentary canal [15,16] and the secretion of pancreatic enzymes [17]. Thus, it triggers the release of some gastrointestinal hormones, enhances the proliferative activity of rat adrenocortical cells and acts as a potent mitogenic agent which displays a growth factor activity for human small-cell lung carcinomas [18]. Because of this wide spectrum of biological activities, there is a considerable interest in the clinical potential of both the agonist and antagonist molecules of bombesin, particularly in the fight against cancer [19,20]. Also, due to its role in the control of appetite, metabolism, and chronic itching they are interesting targets for drug discovery [21,22]. However, in order to develop new drugs a deeper understanding of its structure–activity relationships is necessary.

In regard to the known structure–activity relationships of bombesin, it was early identified that the fragment 6–14 is the shortest sequence retaining full agonist activity, identifying residues Gln^{7}, Trp^{8} and His^{12} to be important for its biological activity. Spectroscopic studies including NMR [23–27], infrared (IR) [28], circular dichroism (CD) and fluorescence spectroscopy [29] and using different solvents like water, dimethylsulfoxide (DMSO) or trifluoroethanol/water mixtures have provided information of the conformational features of bombesin. Specifically, NMR reports in water and DMSO [23–25] describe the structure of bombesin as a random coil. In contrast, NMR experiments of bombesin carried in a trifluoroethanol (TFE)/water mixture (30% v/v) [26,27] report that the C-terminal segment of the peptide ranging from residue 6 to 14 displays a helical conformation, although with residues 11–14 less sharply structured. Moreover, the first two N-terminal residues adopt an extended conformation, while the region between residues 3 and 5 exhibits a great deal of flexibility. The helical feature of the peptide has also been confirmed by IR [28], CD and fluorescence studies [29] when the peptide is incorporated into lipid environments. On view of these results it has been suggested that the C-terminal region of the molecule displays a helical structure into the hydrophobic lipid environment, whereas the rest of the molecule in the aqueous phase exists in a less ordered structure.

2. Computational methods

We intend to contrast the outcome of present simulations with the results of a NMR of bombesin in a mixture TFE/water. The former is a structuring solvent, whose inducing secondary structure capability is thought to be due to the formation of a molecular coating around the peptide such that, intramolecular interactions are enhanced and intermolecular interactions with the solvent are weakened [27,30]. Accordingly, implicit solvent models can be considered as a good approximation in the present case, allowing the peptides to achieve equilibrium faster with the corresponding savings of computer time. Specifically, the Generalized Born/surface area (GB/SA) procedure was selected to treat the solvent in the present work since it offers higher computational efficiency and readily allows for the analytical evaluation of forces [31,32]. Consistently with this choice, the AMBER ff96 force field [33] was selected for the computation of the energy. This selection is based on the results reported by several authors suggesting that the ff96 set reproduces accurately the results of explicit solvent simulations when used with implicit solvent models [34–37]. Accordingly, ff96 parameters were developed for the pyroglutamic residue. Specifically, RESP charges were calculated by fitting the electrostatic potential computed at the Hartree–Fock level with a 6-31G(d) basis set following the Merz–Kollman procedure [38] and using two minimum energy conformations in the fitting procedure.

In the simulations the C-terminal of peptide was amidated while N-terminal was used without any protecting group. Side chains of Glu and Arg residues were considered charged. Salt concentration was set to 0.2 M in order to mimic physiological conditions. An initial extended structure of the peptide was used and energetically minimized with a convergence criterion of 0.005 kcal mol^{-1} $Å^{-1}$. The SHAKE algorithm was used for bonds involving hydrogen atoms and an integration time-step of 2 fs was employed. All the calculations reported in the present work were carried out with the AMBER 9.0 suite of programs [39].

2.1. MD simulations using the GB/SA method and Langevin and Berendsen thermostat algorithms

Starting from the extended conformation, two 200 ns MD simulations using Langevin's and Berendsen's thermostats respectively were performed at 300 K temperature using the Onufriev, Bashford and Case (OBC) implementation of the Generalized Born approximation [40]. Internal dielectric constant in the peptide was set to 1, while an external dielectric constant of 80 corresponding to water was employed.

2.2. REMD simulations

Starting from the extended conformation of bombesin, 100 ns REMD calculations was performed using the OBC implementation of the Generalized Born approximation [40]. The dielectric constant of the peptide (internal dielectric constant) was set to 1 and the external dielectric constant was set to 80, corresponding to water. Prior to the REMD simulations, five standard MD simulations were run during 5 ns at different temperatures ranging from 250 to 750 K to obtain the average value of the energy of the system. Time step was set to 0.2 fs, and SHAKE method was used to constrain all hydrogen atoms. The results of these calculations were used to compute the temperature of the 14 replicas of the present calculation by setting swapping probability of 0.2 and using the condition to have one replica at 300 K. The replicas temperatures used in the present calculation were 280, 300, 321, 344, 369, 395, 424, 454, 487, 523, 561, 603, 648 and 697 K. Replicas were allowed to swap every 2 ps. The temperature during MD simulations was regulated by Langevin's thermostat [9]. Similar kind of analysis as performed for MD simulations, described above, was employed for the REMD collection of configurations.

2.3. Classification of structures (CLASICO)

Analysis of all trajectories was carried out using CLASICO software [41] which permits to monitor the formation/destruction of secondary structures during the folding process, as well as the characterization of the group of structures that represent the folded molecule. The characterization of secondary structures for each of the trajectories was carried out using the procedure reported previously [42]. This procedure also permits the identification of different conformational patterns attained by the peptide, as well as to compare differences of the conformational space sampled using different computational methods.

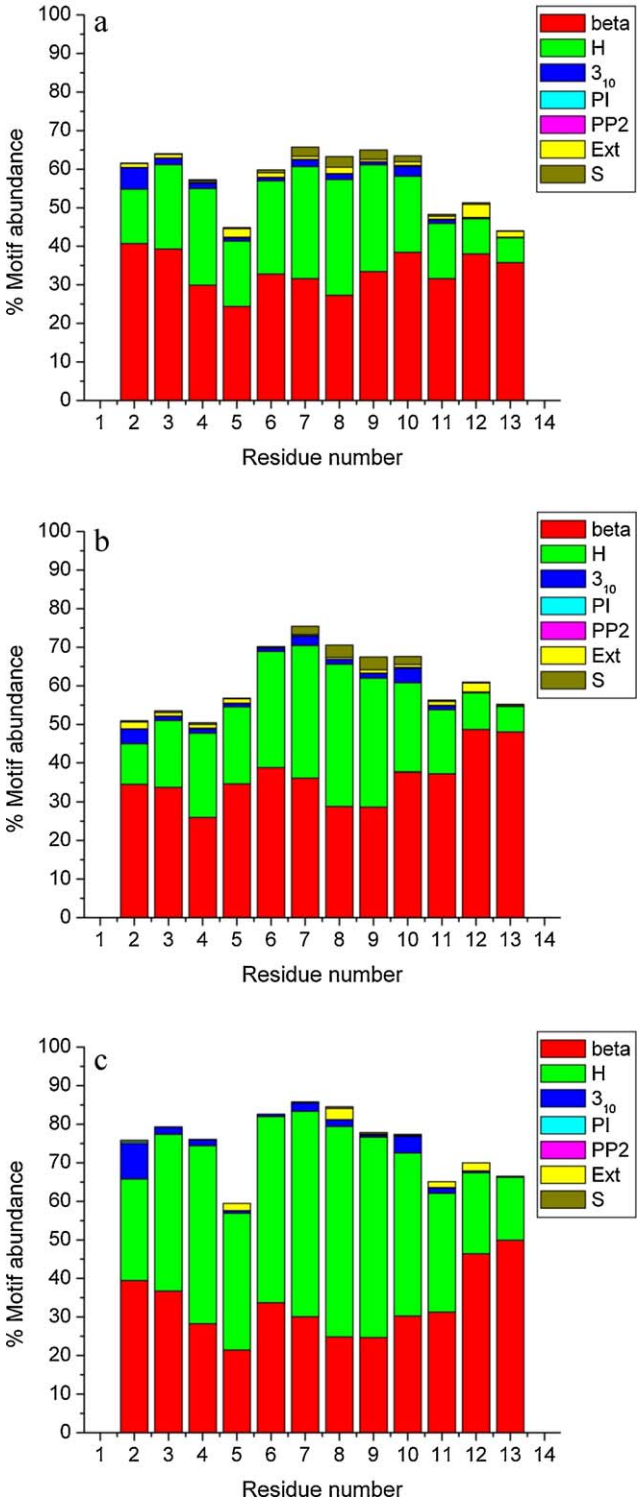

Fig. 1. Motif abundance for the bombesin in (a) MD^{Lang} (b) MD^{Beren} and (c) REMD trajectories. Conformational motifs are labeled: H (α-helix), 310 (310-helix), PI (π-helix), PP2 (polyproline II), EXT (extended), S (β-strand), b (β-turn). Only H, 310 and EXT are exhibited by the structures in the current MD studies.

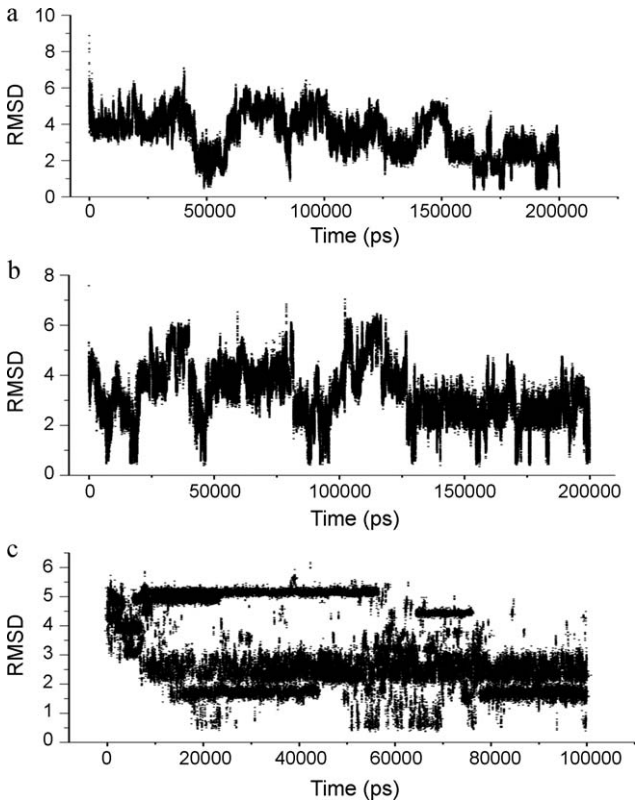

Fig. 2. Main-chain RMSDs of the backbone atoms from the reference structure for (a) MD^{Lang}, (b) MD^{Beren} and (c) REMD, trajectories.

3. Results and discussion

In order characterize the structural features of bombesin we first performed a qualitative analysis of the secondary motifs that can be identified from the three protocols tested. For this purpose we used the in-house program CLASICO that permits to identify secondary motifs from each snapshot, as described elsewhere [42]. The program translates each snapshot into a string of letters according to the following procedure: proceeding in a sequential manner, the program computes for each residue its backbone dihedral angles and assigns a letter to it following the Zimmerman partition of the Ramachandran map [43]. Following a set of rules, each string is analyzed using a three-letter window to assign the corresponding secondary motif. Histograms of the secondary motifs per residue for each of the three procedures used in the present work are depicted in Fig. 1a–c. It should be noted that the CLASICO program [41] does not include first and last residues of the peptide in secondary structure calculations which is why both the residues are not displaying any of the secondary structure features in Fig. 1a–c. As can be seen, from the figures the three profiles are very similar. They show the peptide very structured: about 60–70% for the MD calculations whereas for the REMD calculation is about 80%. As can be seen, all three calculations predict a high helical content for the whole sequence, being higher between residues 6 and 10. It can also be appreciated a lower degree of structuration at positions 5 and 11 as expected since these positions are occupied by glycine residues. In order to understand the differences of the different procedures, the histograms need to be compared pairwisely. The difference in helix content found between the REMD calculation (Fig. 1c) and the MD trajectory performed using the Langevin thermostat (Fig. 1a) must be due to a different sampling time and that the sampling is temperature biased. On the other hand, the MD performed using the Berendsen thermostat (Fig. 1b) in comparison to the one performed using the Langevin thermostat (Fig. 1a) shows differential behavior in regard to the N-terminus. Thus, whereas the latter predicts a helical structure, the former, indicates lesser content and even a clear sampling as extended, closer to the NMR experiments.

In order to get insight into the structural features of the peptide we picked up a helical structure from set of configurations sampled

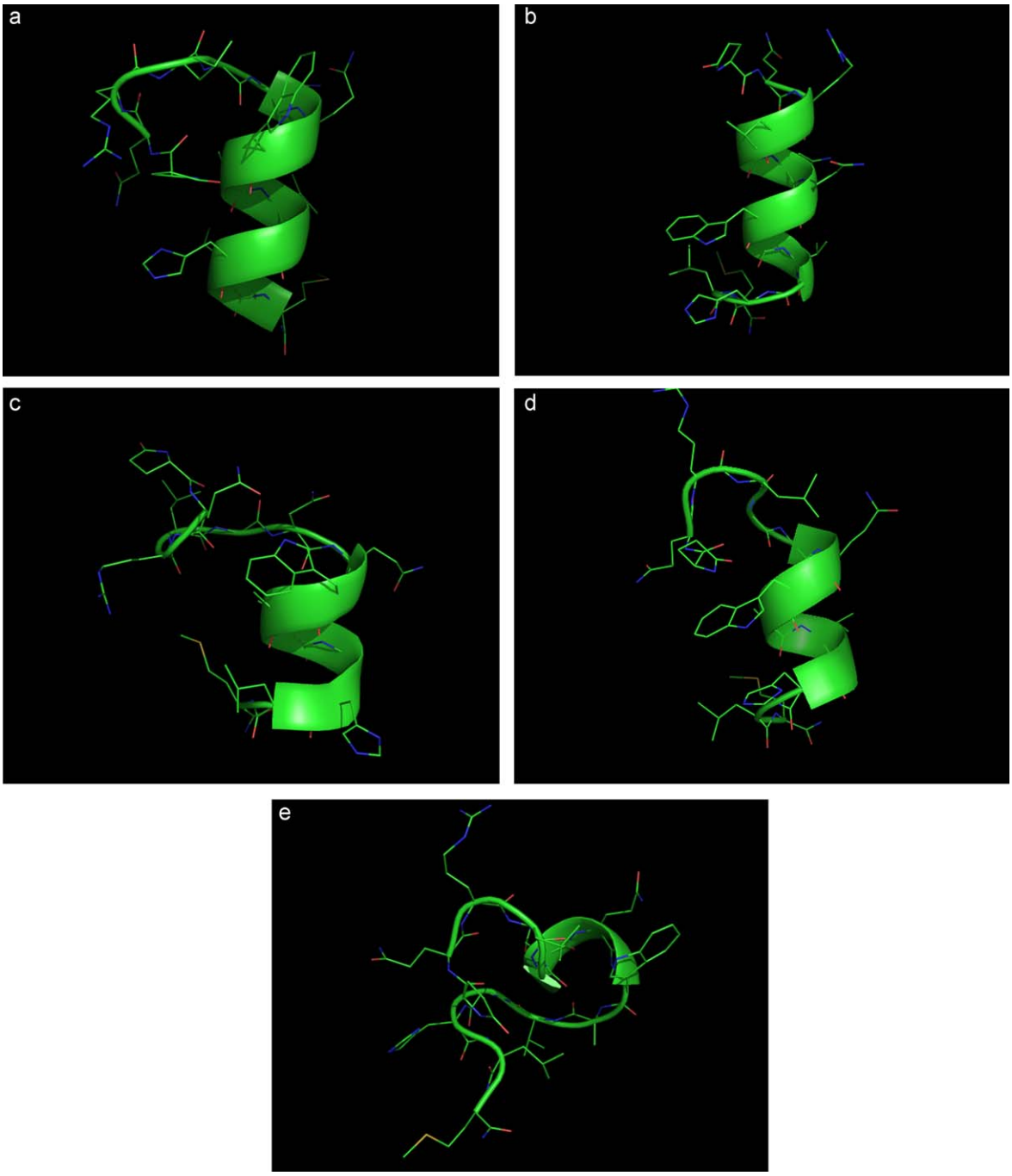

Fig. 3. Average structures of the different intervals (a–d) classified according to the rmsd to a helical structure between residues 6 and 10.

and it was considered as reference. Then, we computed the root-mean-square deviation (rmsd) of each of the snapshots in regard the reference structure and plotted along the sampling process. Fig. 2a–c shows pictorially the values obtained. The two MD trajectories show a continuum, not observed in the REMD calculation, since the produced sampling in this method does not correspond to a temporal series. The snapshots were then classified into five sets according to the rmsd to the reference structure: set#1 rmsd ≤ 1; set#2 $1 \leq$ rmsd ≤ 2; set#3 $2 \leq$ rmsd ≤ 3; set#4 $3 \leq$ rmsd ≤ 4; set#5 $4 \leq$ rmsd ≤ 7. The percentage of structures in each of the sets is: for the REMD calculation, 21%; 44%; 8%, 2%; 25%; MD (Langevin), 10%, 27%, 61%, 2%, 0%; MD (Berendsen), 8%, 36%, 45%, 2%, 9%. The average structures of the different sets are shown pictorially in Fig. 3. The average structure of set#1 exhibits a well defined α-helical structure on the segment ranging from residue 6 to 14. At the N-terminus on the other hand, the structure exhibits a type I β-turn between residues Glu^2 and Gly^5. Set#2 exhibits also a helical structure between residues 6 and 14 although modified into a π-helix in its C-terminus. This may cause decrease of stability that must be compensated by the favorable interaction of the aromatic side chains of Trp^8 and His^{12} that are aligned. This is an interesting structural feature, since these two residues are known to be important in the activity of the peptide, so that being on the same side of the helix, may be connected to its recognition with the receptor surface. At the N-terminus the structure also exhibits a type I β-turn between residues Glu^2 and Gly^5. In regard to set#3, the interaction between the side chains of Glu^2 and Asn^6 disrupts the helical structure at residues 6 and 7, although this compensated with a

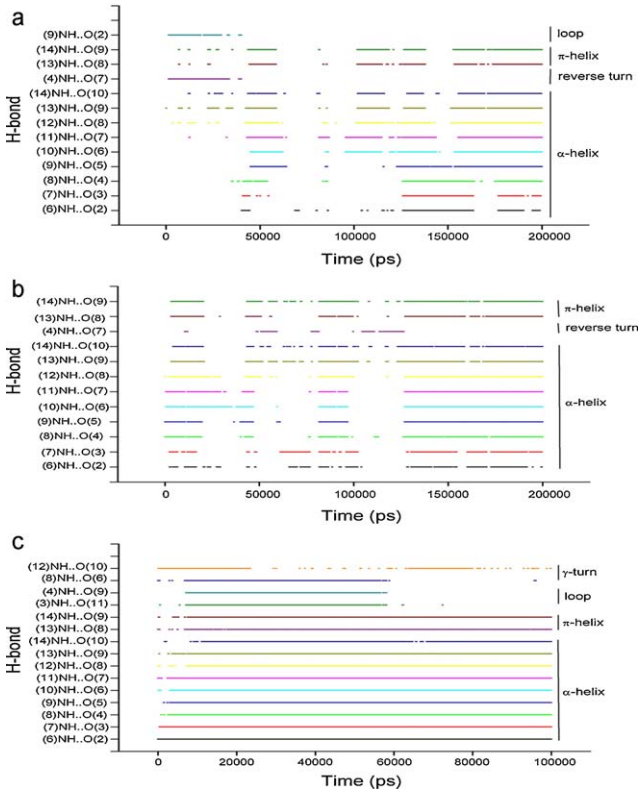

Fig. 4. Progress of hydrogen bonds monitored between important residues for bombesin in (a) MD^{Lang} (b) MD^{Beren} and (c) REMD trajectories. Secondary structures (α-helix, π-helix, turns, loop etc.) are assigned in terms of hydrogen bonding between the different residues in the peptide.

type I β-turn between residues Glu^2 and Gly^5. In this structure the helix is distorted at the C-terminus. Set#4 exhibits a helical structure between residues 6 and 14 although with the last two turns exhibiting a π-helix. This structure shows again the favorable interaction between residues Trp^8 and His^{12}. Moreover, in its structure the N-terminus exhibits a bent conformation. Finally, set#5 clearly deviates from the helical structure, although with frequent turn conformations especially around the segment Gly^5-Ala^9 as will be discussed later.

These observed tendencies in the secondary structure can be further rationalized through the analysis of the backbone–backbone hydrogen bonding. The statistical analysis of the hydrogen bonds (HBs) observed during the sampling process for the different calculations is shown in Table 1. The geometrical criterion used to consider two atoms – donor (A) and acceptor (B) – in a HB were to have a distance is equal or less than 3.0 Å and angle HAB (<HAB) is considered equal or less than 120°. In order to obtain significant results, only the hydrogen bond with a percentage of existence equal or greater than 1.0% is considered during the simulation time. Moreover, the hydrogen atoms of both terminals –NH2 groups are considered indistinguishable.

Table 1 lists the type of interactions and the percentage of the conformations appeared in the currently investigated simulations, calculated in terms of backbone–backbone hydrogen bonding. Although most of the conformations sampled in each of the trajectories correspond to α-helical (residues 2–14) REMD has proven to be better in sampling the helical conformations (Table 1). Among other observations, these results demonstrate that two β-turns between residues 6 and 8 and 10 and 12 along with two loops between residues 3 and 11 and 4 and 9 have been sampled in $REMD^{Lang}$, whereas they were absent in MD^{Lang} and MD^{Beren} trajectories. On the contrary, no reverse turns were observed in REMD while they were found in the MD^{Lang} and MD^{Beren} simulations between 4 and 7 residues.

Fig. 4a–c shows diagrammatically the prevalence of difference hydrogen bonding patterns along the sampling process. Although all three diagrams provide an image of the frequency hydrogen bonding structures are sampled as well as when they are exhibited simultaneously, in the case of Fig. 4a and b they also represent the time evolution of HB formation and breaking. Specifically, in the case of the MD trajectory performed using the Langevin thermostat (Fig. 4a), HBs responsible for its helicity are almost negligible till 40 ns, when the helical region between residues 5 and 10 can be observed during the next 20 ns. The region between 105 and 200 ns of trajectory, excluding the segment between 165 and 178 ns, samples conformations with helical structure between residues 6 and 14. A hydrogen bond between residues 2 and 9 corresponding to a loop conformation was also observed in some of the structures sampled during initial 30 ns of the trajectory. The corresponding HB diagram for the trajectory performed using the Berendsen thermostat is shown in Fig. 4b. In this case, helical conformations are sampled from the beginning of trajectory. The segments of trajectory showing regular distribution of hydrogen bonds and accounting for helical structures between residues 2 and 14 can be distinguish in the intervals 1–5, 11–18, 82–84 and 123–200 ns. To some extent hydrogen bonding between 8 and 13 and 9 and 14 residues responsible for π-helical structure was also sampled mainly in the intervals 5–15, 130–158 and 170–200 ns. Finally, Fig. 4c shows the hydrogen bonding pattern in the sampling process using the REMD method. Inspection of the figure reveals the extensive appearance of hydrogen bonds between residues 2 and 14. The existence of two π-helical turns between 8 and 13 and 9 and 14 residues can also be observed in most of the conformations. Two consistent hydrogen bonds between 6 and 8 and 10 and 12 residues corresponding to β-turn were also observed in most of the configuration sampled. Overall, these results suggest that peptide has high propensity to adopt helical conformations flanked by residues 2–14, under REMD conditions.

Finally, it is a good exercise to compare the results with the aggregated information provided from the NMR spectrum. Since the NOE intensities of a NMR spectrum are inversely related to the six power of the distance between the atoms involved, distances computed from the NMR spectrum are directly comparable with the results of the simulations. In order to compare the results of the present calculations with the experimental data available, we took eight long distance NOEs from the NMR spectrum recorded in TFE/water [27]. These signals can be classified according to its intensity as strong (s), medium (m), weak (w) and very weak (vw) [44]. The intensity of the signal provides a range for the corresponding atom-atom distances [45]. The NOEs considered are in the present study include: (i) C^{α}–N between Gln^7-Val^{10} (m), Trp^8-Gly^{11} (w), Ala^9-His^{12} (w), Val^{10}-Leu^{13} (m) and Gly^{11}-Met^{14} (w); (ii) a C^{α}–N between Gln^7-Gly^{11} (m) and iii) C^{α}–C^{α} Asn^6-Ala^9 (vw) and Val^{10}-Leu^{13} (vw) [27]. Independently the distances between the corresponding atoms responsible for the different experimental NOEs were computed from the different calculations performed in the present study. Distances are reported as the average of the distance computed for each snapshot with a tolerance factor of ±1.96 standard deviations, covering a 95% of the variance assuming that they exhibit a normal distribution.

Figs. 5–7 show pictorially the overlapping between experimental and computed distances for the MD^{Lang} and MD^{Beren} and REMD calculations, respectively. If we compare the different boxes of one calculation, all three figures show the same pattern: there is good overlap between NMR results and computations for the structures of intervals 1–3 and partial overlap for the structures of interval 4, whereas for the structures of interval 5 the overlap is negligible. In the case of the structures of sets 1–3 the overlap of the

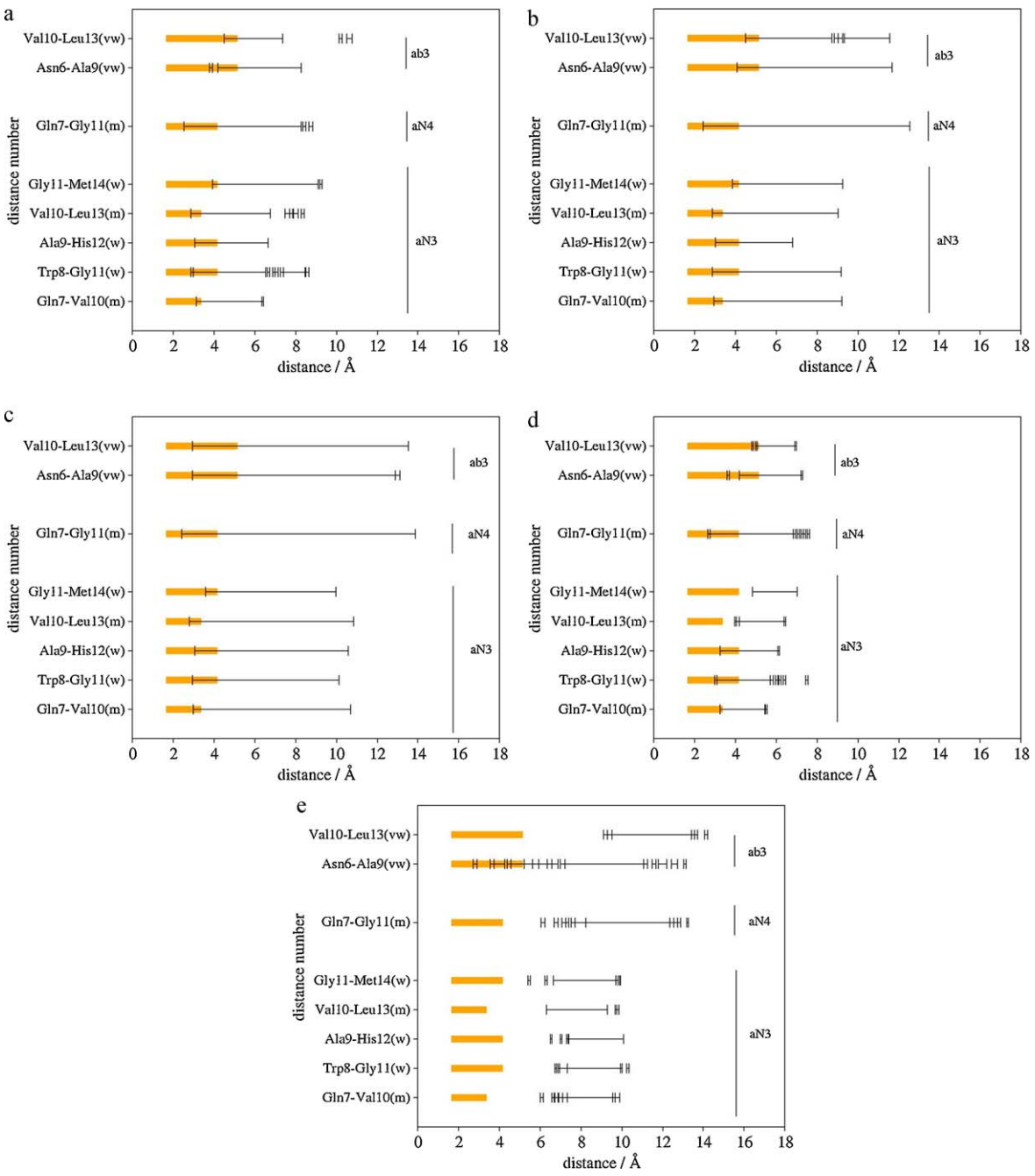

Fig. 5. Comparison of reported NMR distances shown in orange and the MD^{Lang} average with the distance intervals (1–5) containing 95% structures during the MD^{Lang} sampling process.

computed distances and the NOE derived distances is similar. Looking at Fig. 3 we can see that the structures belonging to these sets exhibit in common a helical structure along the segment 6–14 that correlates well with the observed distances derived from the NMR spectrum. However, there are differences in the dispersion of different distances sampled during the simulations and can be observed in all the three calculations. Specifically, comparison of Fig. 7a and b shows a larger dispersion of the distances Gly^{11}-Met^{14} and Gln^{7}-Gly^{11} in the latter, that is extended to all the distances when Fig. 7b and c are compared. This larger fluctuations of distances located at the C-terminus can be associated with deviations from the α-helical structure at the edge of the peptide, as can be seen from inspection of the average structures shown in Fig. 3a–c. In fact, these deviations can be associated with the formation of a π-helix, as shown at last turn of the structure of Fig. 3b. This is corroborated by the appearance of a HB between $Trp^{8}CO\cdots NHLeu^{13}$ and $Ala^{9}CO\cdots NHMet^{14}$, shown in the HB analysis listed in Table 1. In contrast, structures belonging to interval 4 do not fulfill the NMR derived distances Val^{10}-Leu^{13} and Gly^{11}-Met^{14}. As can be seen in Fig. 3d these structures do not show helicity at the C-terminus.

This analysis stands for the commonalities between the three simulations performed in the present work; however there are also differences in the results provided among them. Specifically, the dispersion of the distance for the structures classified in intervals 3, 4 and 5 are similar in the three calculations. In contrast, this dispersion is larger for the Langevin simulation in the two first intervals (Figs. 5–7a and b), whereas for REMD and Berendsen provide similar results. Thus, comparison of the results obtained in the two MD simulations, suggests that the thermostats must play a role in the sampling process. Indeed, inspection of the rmsd from a 6–14

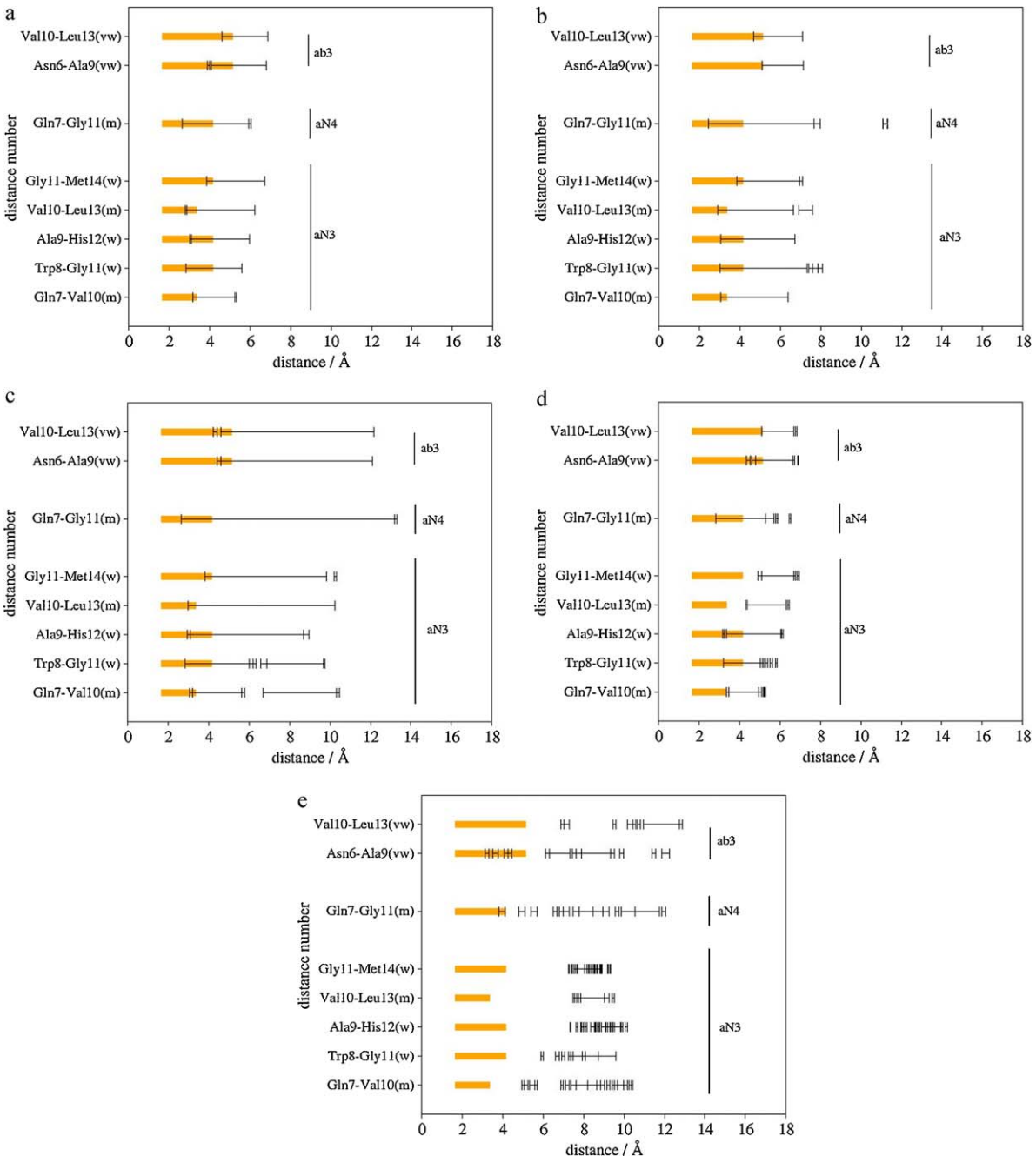

Fig. 6. Same as Fig. 5 for the MD^{Beren} trajectory.

helical structure (Fig. 2) suggests that the peptide samples more frequently the folded conformation using Berendsen's thermostat compared to Langevin's thermostat. This is due to an observed biasing effect of former to enhance folded structures [46]. Now, comparing REMD calculations with MD using the Langevin's thermostat, it can be suggested that the better fulfillment of the NMR results of the former, is due to the known extremely quick process of equilibration observed in the REMD calculations [47] that is reflected in the number of configurations sampled in intervals 1 and 2 as compared with the MD simulations.

Let us now sketch a few structure–activity results in view of the structural results reported in the present work. Results clearly show that the peptide attains a helical structure on the segment 6–14 regardless of the methodologies used. Moreover, the helical structure exhibits a tendency to unwind at the C-terminus showing a propensity to adopt a π-helix at its last turn. This behavior is related to the presence of two glycines at strategic positions 5 and 11, a helix breaker residue. So, Gly^5 acts as a hinge between the N-terminus and the rest of the chain, whereas Gly^{11} perturbs the helix at the C-terminus. These structural features help to explain the known biological data. On the one hand, the fragment 6–14 of bombesin is known to be the shortest fragment retaining activity. This fact can be correlated with the clear tendency of the peptide to adopt a helical structure along this region of the peptide. Indeed, analogs containing residues with a helical inducer like α-aminoisobutyric acid (Aib), exhibit enhanced affinity [48,49]. Moreover, since residues Gln^7, Trp^8 and His^{12} are important for bombesin activity, they may thought to play a role stabilizing the helical secondary structure and/or in the recognition process with the receptor through their side chains. Let consider first the role of

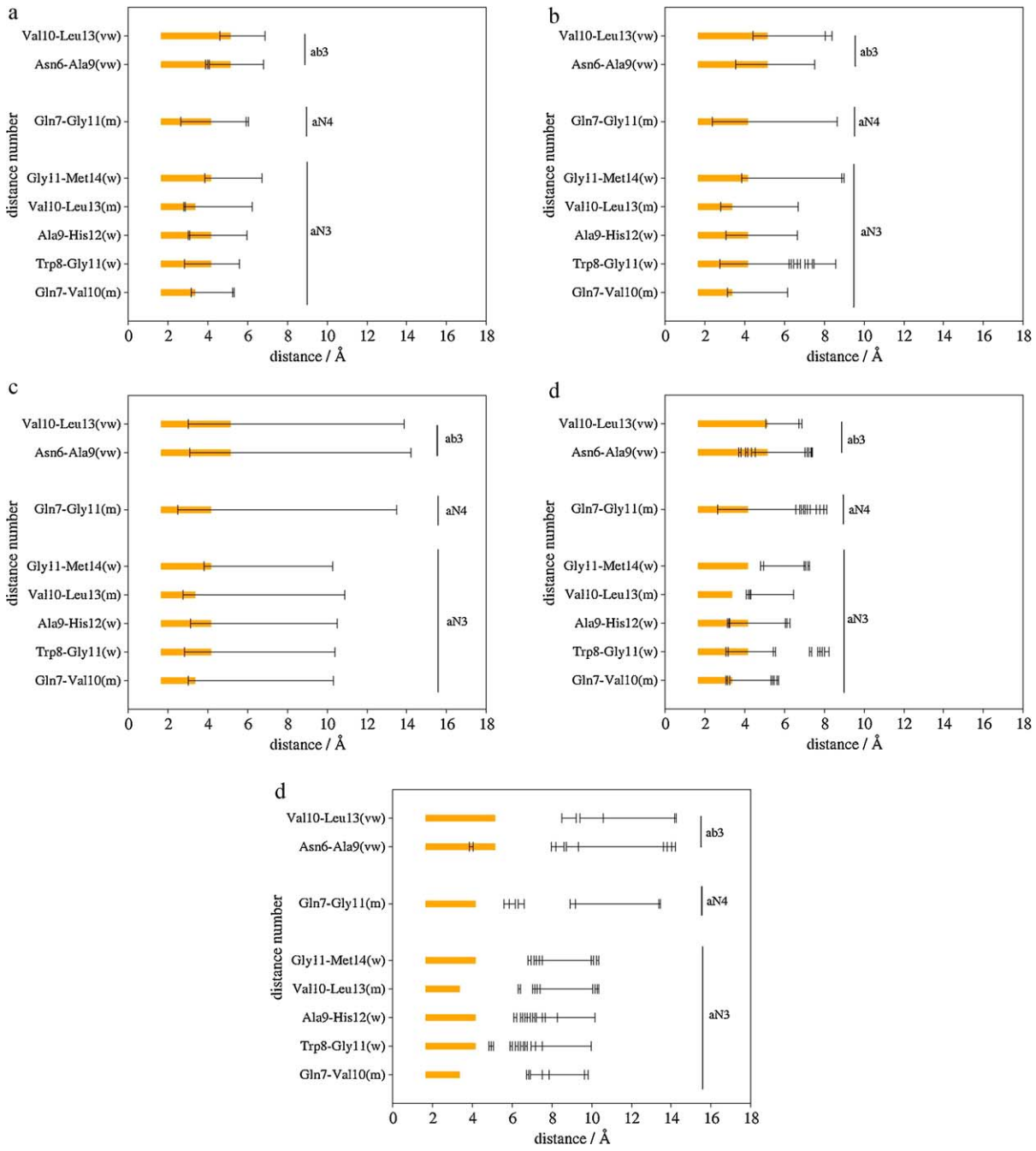

Fig. 7. Same as Fig. 5 for the REMD trajectory.

Trp[8] and His[12]. Analysis of the trajectories reported in the present work reveal that the distance between these two side chains moves between 4 Å and 9 Å about 50% each. When the two side chains get closer they form a π–π stacking interaction (see Fig. 8a), providing a structural support for the helical structure and possibly a role in the recognition to the receptor. When the two side chains get apart, when they are at the longest distance the helix gets distorted at the C-terminus. On the other hand, the analysis of the calculations reported in the present work also shows that Gln[7] and Trp[8] side chains are involved in a NH···π hydrogen bond during about 40% of the trajectories (Fig. 8b). This interaction reinforces the structure of a helix turn between residues Gly[5] and Ala[9], stabilized by the corresponding carbonylamide backbone hydrogen bond (see Table 1). In this situation the helix is distorted, preventing the interaction between the two aromatics side chains Trp[8] and His[12]. Accordingly, the dynamical picture emerging is that Trp[8] plays a role of a hinge, reinforcing the helical structure on the one hand through a π–π interaction and stabilizing the Gly[5]-Ala[9] helical turn on the other. The reinforcing role of Gln[7] on the helix turn can be further justified taking into account that when is substituted by a histidine as in Neuromicin C, the peptide exhibits no significant loss of biological activity to the BB2 receptor, but is losses two orders of magnitude binding to the BB1 receptor. This could be explained if we consider that His is a poorer helical inducer than Gln and consequently, the peptide may lose part of it intrinsic tendency to form a helix, but can form a hydrogen bond with the Trp side chain as Gln does. This doble capability could explain the dual pharmacological behavior of the peptide in regard receptors BB1 and BB2. However, further investigation needs to be done in this direction.

Table 1
Hydrogen bonds observed between backbone atoms and their residence times (in percentage of observance in regard to the total of snapshots).

No.	Definition	Secondary structure	MD^{Lang}	MD^{Beren}	$REMD^{Lang}$
1	$(Gln^2)CO\cdots NH(Asn^6)$	α-Helix	8.9	8.8	22.0
2	$(Arg^3)CO\cdots NH(Gln^7)$	α-Helix	7.3	12.4	21.7
3	$(Leu^4)CO\cdots NH(Trp^8)$	α-Helix	11.9	17.4	29.2
4	$(Gly^5)CO\cdots NH(Ala^9)$	α-Helix	16.4	16.7	39.3
5	$(Asn^6)CO\cdots NH(Val^{10})$	α-Helix	10.5	11.0	24.4
6	$(Gln^7)CO\cdots NH(Gly^{11})$	α-Helix	12.3	13.5	24.3
7	$(Trp^8)CO\cdots NH(His^{12})$	α-Helix	15.0	19.6	32.0
8	$(Ala^9)CO\cdots NH(Leu^{13})$	α-Helix	8.2	9.2	18.0
9	$(Val^{10})CO\cdots NH(Met^{14})$	α-Helix	6.0	6.1	16.0
10	$(Gln^7)CO\cdots NH(Leu^4)$	β-Turn	7.5	5.8	–
11	$(Trp^8)CO\cdots NH(Leu^{13})$	π-Helix	5.4	7.1	9.1
12	$(Ala^9)CO\cdots NH(Met^{14})$	π-Helical	9.2	12.7	16.3
13	$(Gln^2)CO\cdots NH(Ala^9)$	Loop	5.6	–	–
14	$(Gly^{11})CO\cdots NH(Arg^3)$	Loop	–	–	7.7
15	$(Ala^9)CO\cdots NH(Leu^4)$	Loop	–	–	5.4
16	$(Asn^6)CO\cdots NH(Trp^8)$	β-Turn	–	–	6.1
17	$(Val^{10})CO\cdots NH(His^{12})$	β-Turn	–	–	5.27

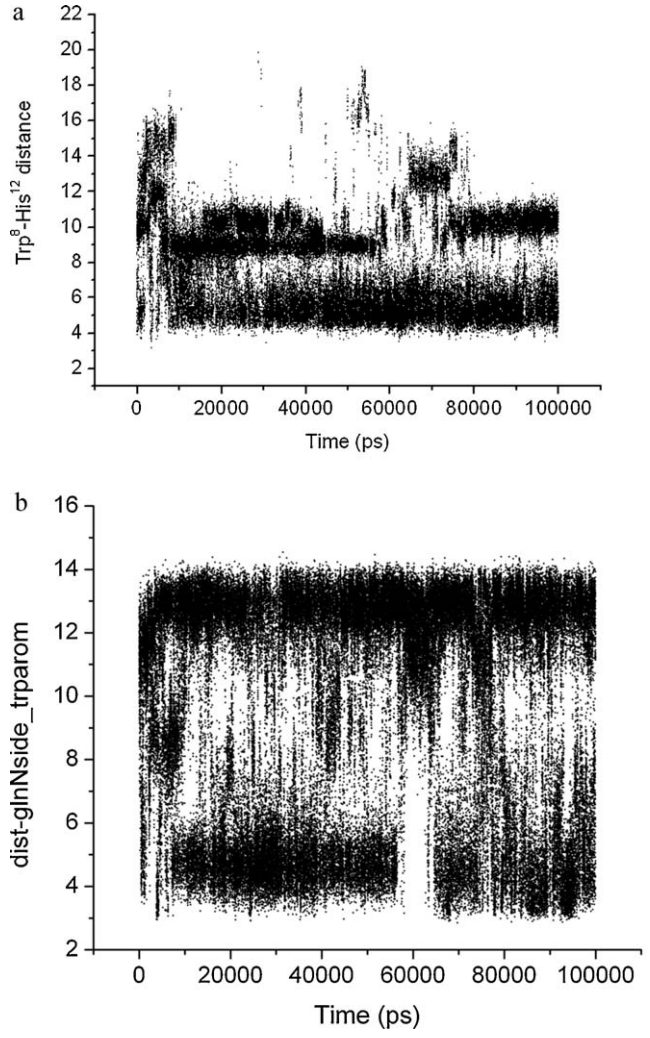

Fig. 8. (a) Distance between the centers of the aromatic rings of Trp^8 and His^{12} during the REMD sampling process; (b) values of the distance between the amide group of the Gln^7 side chain and the center of the aromatic ring of Trp^8 during the RMED sampling process.

4. Conclusions

The present investigations involve the utilization and comparison of two 200 ns MD trajectories (using Langevin and Berendsen thermostats, respectively) and a 100 ns REMD sampling process to explore the conformational space of bombesin using the OBC implementation of the GB method to describe the solvent. Calculations were carried out using the AMBER ff96 force field, considered to be adequate to use in combination with implicit solvent methods [34–37]. The results obtained clearly show that the peptide attains a helical structure on the segment 6–14 regardless of the methodologies used. This result is clearly connected to the activity of the peptide, since it is known that the bombesin fragment 6–14 is the shortest fragment retaining activity. Moreover, the results also show the tendency of the peptide to adopt a π-helix at the C-terminus aligning the aromatic residues Trp^8 and His^{12}. On the other hand, side chain of Gln^7 is found to form a NH–π hydrogen bond with the side chain of Trp^8 distorting the helix at its C-terminus, suggesting that Trp^8 plays a role of a hinge winding and unwinding the helical C-terminus of the peptide. In regard to the methodological aspects of present results, although the three methodologies provide the same general conclusion, the REMD is more robust for the purpose of sampling, providing less uncertainty as measured through the fulfillment of the NMR results as compared with MD simulations [48,49]. MD^{Beren} shows a bias to sample folded structures in comparison to the MD^{Lang}. Moreover, taking into account that the REMD calculations were done using the Langevin thermostat, direct comparison to MD^{Lang} demonstrates the quick equilibration process being undertaken when using the REMD procedure.

Acknowledgements

Financial support provided by the Spanish–South African Research Partnership Program through grant number 2075517 (HS2006-0022) is gratefully acknowledged. A PDF fellowship awarded by the NRF and DUT is gratefully acknowledged by Dr. P. Singh. This work is supported by the Spanish Ministry of Science and innovation through the grant SAF2008-04943-C02-01.

References

[1] S. Honda, T. Akiba, Y.S. Kato, Y. Sawada, M. Sekijima, M. Ishimura, A. Ooishi, H. Watanabe, T. Odahara, K.J. Harata, Crystal structure of a ten-amino acid protein, J. Am. Chem. Soc. 130 (2008) 15327–15331.
[2] M. Buck, Trifluoroethanol and colleagues: cosolvents come of age. Recent studies with peptides and proteins, Q. Rev. Biophys. 31 (1998) 297–355.
[3] A. Liwo, C. Czaplewski, S. Oldziej, H.A. Scheraga, Computational techniques for efficient conformational sampling of proteins, Curr. Opin. Struct. Biol. 18 (2008) 134–139.
[4] F.J. Corcho, M. Filizola, J.J. Perez, Evaluation of the iterative simulated annealing technique in conformational search of peptides, Chem. Phys. Lett. 319 (2000) 65–70.

[5] H.A. Scheraga, M. Khalili, A. Liwo, Protein-folding dynamics: overview of molecular simulation techniques, Ann. Rev. Phys. Chem. 58 (2007) 57–83.
[6] J.J. Perez, H.O. Villar, G.A. Arteca, Distribution of conformational energy minima in molecules with multiple torsional degrees of freedom, J. Phys. Chem. 98 (1994) 2318–2324.
[7] X. Daura, B. Jaun, D. Seebach, W.F. van Gustaren, A.E. Mark, Reversible peptide folding in solution by molecular dynamics simulation, J. Mol. Biol. 280 (1998) 925–932.
[8] H.J.C. Berendsen, J.P.M. Postma, W.F. van Gunsteren, A. DiNola, J.R. Haak, Molecular-dynamics with coupling to an external bath, J. Chem. Phys. 81 (1984) 3684–3690.
[9] R.W. Pastor, B.R. Brooks, A. Szabo, An analysis of the accuracy of langevin and molecular-dynamics algorithms, Mol. Phys. 65 (1988) 1409–1419.
[10] Y. Sugita, Y. Okamoto, Replica-exchange molecular dynamics method for protein folding, Chem. Phys. Lett. 314 (1999) 141–151.
[11] A. Anastasi, V. Erspamer, M. Bucci, Isolation and structure of bombesin and alytesin, 2 analogous active peptides from skin of European amphibians bombina and alytes, Experientia 27 (1971) 166–167.
[12] V. Erspamer, G. Improta, P. Melchiorri, N. Sopranri, Evidence of cholecystokinin release by bombesin in dog, Br. J. Pharmacol. 52 (1974) 227–232.
[13] R. Bruzzone, Mechanism of action of bombesin on amylase secretion – evidence for a Ca^{2+}-independent pathway, Eur. J. Biochem. 179 (1989) 323–331.
[14] V. Erspamer, P. Melchiorri, Active polypeptides – from amphibian skin to gastrointestinal-tract and brain of mammals, Trends Pharmacol. Sci. 1 (1980) 391–395.
[15] E.A. Mayer, J.R. Reeve Jr., S. Khawaja, P. Chew, J. Elashoff, B. Clark, J.H. Walsh, Potency of natural and synthetic canine gastrin-releasing decapeptide on canine antral muscle, Am. J. Physiol. 250 (1986) G581–G587.
[16] C. Herrmann, J.C. Cuber, T. Dakka, C. Bernard, J.A. Chayvialle, Bombesin potentiates taurocholic acid-induced neurotensin release in rats, Endocrinology 128 (1991) 2853–2857.
[17] R.W. Alexander, J.R. Upp, G.J. Poston, V. Gupta, C.M. Townsend Jr., J.C. Thompson, Effects of bombesin on growth of human small cell lung-carcinoma in vivo, Cancer Res. 48 (1988) 1439–1441.
[18] M.E. Sunday, N. Choi, E.R. Spindel, W.W. Chin, E.J. Mark, Gastrin-releasing peptide gene expression in small-cell and large cell undifferentiated lung carcinomas, Hum. Pathol. 22 (1991) 1030–1039.
[19] S. Mahmoud, J. Staley, J. Taylor, A. Bogden, J.-P. Moreau, D. Coy, I. Avis, F. Cuttitta, J.L. Mulshine, T.W. Moody, [Psi13,14] Bombesin analogs inhibit growth of small-cell lung-cancer in vitro and in vivo, Cancer Res. 51 (1991) 1798–1802.
[20] Y. Qin, T. Ertl, R.-Z. Cai, G. Halmos, A.V. Schally, Inhibitory effect of bombesin receptor antagonist rc-3095 on the growth of human pancreatic-cancer cells in-vivo and in-vitro, Cancer Res. 54 (1994) 1035–1041.
[21] Z. Merali, J. McIntosh, H. Anisman, Role of bombesin-related peptides in the control of food intake, Neuropeptides 33 (1999) 376–386.
[22] K. Yamada, E. Wada, Y. Santo-Yamada, K. Wada, Bombesin and its family of peptides: prospects for the treatment of obesity, Eur. J. Pharmacol. 440 (2002) 281–290.
[23] J.A. Carver, The conformation of bombesin in solution as determined by two-dimensional ^{1}H-NMR techniques, Eur. J. Biochem. 168 (1987) 193–199.
[24] J.A. Carver, A two-dimensional ^{1}H-NMR study of the solution conformation of gastrin releasing peptide, Biochem. Biophys. Res. Commun. 150 (1988) 552–560.
[25] C. DiBello, L. Gozzini, M. Tonellato, M.G. Corradini, G. D'Auria, L. Paolillo, E. Trivellone, 500 MHz NMR characterization of synthetic bombesin and related peptides in DMSO-d_6 by two-dimensional techniques, FEBS Lett. 237 (1988) 85–90.
[26] J.A. Carver, J.G. Collins, NMR identification of a partial helical conformation for bombesin in solution, Eur. J. Biochem. 187 (1990) 645–650.
[27] M.D. Dìaz, M. Fioroni, K. Burger, S. Berger, Evidence of complete hydrophobic coating of bombesin by trifluoroethanol in aqueous solution: an NMR spectroscopic and molecular dynamics study, Chem. Eur. J. 8 (2002) 1663–1669.
[28] D. Erne, R. Schwyzer, Membrane-structure of bombesin studied by infrared-spectroscopy – prediction of membrane interactions of gastrin-releasing peptide, neuromedin-B, and neuromedin-C, Biochemistry 26 (1987) 6316–6319.
[29] P Cavatorta, G. Farruggia, L. Masotti, G. Sartor, A.G. Szabo, Conformational flexibility of the hormonal peptide bombesin and its interaction with lipids, Biochem. Biophys. Res. Commun. 141 (1986) 99–105.
[30] P. Luo, R.L. Baldwin, Mechanism of helix induction by trifluoroethanol: a framework for extrapolating the helix-forming properties of peptides from trifluoroethanol/water mixtures back to water, Biochemistry 36 (1997) 8413–8421.
[31] W.C. Still, A. Tempczyk, R.C. Hawley, T. Hendrickson, Semianalytical treatment of solvation for molecular mechanics and dynamics, J. Am. Chem. Soc. 112 (1990) 6127–6129.
[32] J. Chen, C.L. Brooks III, J. Khandogin, Recent advances in implicit solvent-based methods for biomolecular simulations, Curr. Opin. Struct. Biol. 18 (2008) 140–148.
[33] P.A. Kollman, R. Dixon, W. Cornell, T. Fox, C. Chipot, A. Pohorille, The development/application of a 'minimalist' organic/biochemical molecular mechanics force field using a combination of *ab initio* calculations and experimental data, Comp. Simul. Biomol. Systems 3 (1997) 83–96.
[34] R. Zhou, Free energy landscape of protein folding in water: explicit vs. implicit solvent, Proteins: Struct., Funct., Bioinf. 53 (2003) 148–161.
[35] D.R. Roe, A. Okur, L. Wickstrom, V. Hornak, C. Simmerling, Secondary structure bias in generalized Born solvent models: comparison of conformational ensembles and free energy of solvent polarization from explicit and implicit solvation, J. Phys. Chem. B 111 (2007) 1846–1857.
[36] M.S. Shell, R. Ritterson, K.A. Dill, A test on peptide stability of AMBER force fields with implicit solvation, J. Phys. Chem. B 112 (2008) 6878–6886.
[37] A. Rodriguez, P. Mokoena, F.J. Corcho, K. Bisetty, J.J. Perez, Computational study of the free energy landscape of the miniprotein CLN025 in explicit and implicit solvent, J. Phys. Chem. B, in press.
[38] U.C. Singh, P.A. Kollman, An approach to computing electrostatic charges for molecules, J. Comp. Chem. 5 (1984) 129–145.
[39] D.A. Case, T.A. Darden, T.E. Cheatham III, C.L. Simmerling, J. Wang, R.E. Duke, R. Luo, K.M. Merz, D.A. Pearlman, M. Crowley, R.C. Walker, W. Zhang, B. Wang, S. Hayik, A. Roitberg, G. Seabra, K.F. Wong, F. Paesani, X. Wu, S. Brozell, V. Tsui, H. Gohlke, L. Yang, C. Tan, J. Mongan, V. Hornak, G. Cui, P. Beroza, D.H. Mathews, C. Schafmeister, W.S. Ross, P.A. Kollman, AMBER 9, University of California, San Francisco, 2006.
[40] A. Onufriev, D. Bashford, D.A. Case, Exploring protein native states and large-scale conformational changes with a modified generalized Born model, Proteins: Struct., Funct., Bioinf. 55 (2004) 383–394.
[41] LaFargaCPL: CLASTERIT: Project Info. Available from: http://devel.cpl.upc.edu/clasterit.
[42] F. Corcho, J. Canto, J.J. Perez, Comparative analysis of the conformational profile of substance P using simulated annealing and molecular dynamics, J. Comput. Chem. 25 (2004) 1937–1952.
[43] S.S. Zimmerman, M.S. Pottle, G. Nemethy, H.A. Scheraga, Conformational-analysis of 20 naturally occurring amino-acid residues using ECEPP, Macromolecules 10 (1977) 1.
[44] J.L. Markley, A. Bax, Y. Arata, C.W. Hilbers, R. Kaptein, B.D. Sykes, P.E. Wright, K. Wuthrich, Recommendations for the presentation of NMR structures of proteins and nucleic acids, J. Mol. Biol. 280 (1998) 933–952.
[45] G. Gasmi, A. Singer, J. Forman-Kay, B. Sarkar, NMR structure of neuromedin C, a neurotransmitter with an amino terminal Cu^{II}-, Ni^{II}-binding (ATCUN) motif, J. Peptide Res. 49 (1997) 500–509.
[46] E. Rosta, N.-V. Buchete, G. Hummer, Thermostat artifacts in replica exchange molecular dynamics simulations, J. Chem. Theor. Comput. 5 (2009) 1393–1399.
[47] B. Cooke, S.C. Schmidler, Preserving the Boltzmann ensemble in replica-exchange molecular dynamics, J. Chem. Phys. 129 (2008) 164112.
[48] S. Prasad, A. Mathur, N. Gupta, M. Jaggi, A.T. Singh, P. Rajendran, V.K. Sanna, R. Mukherjee, Bombesin analogs containing α-amino-isobutyric acid with potent anticancer activity, J. Pept. Sci. 13 (2007) 54–62.
[49] A. Rodriguez, J. Canto, F.J. Corcho, J.J. Perez, Computational investigation of the conformational profile of the four stereomers of Ac-L-Pro-c3Phe-NHMe (c3Phe = 2,3-methanophenylalanine), Biopolymers (Pept. Sci.) 92 (2009) 518–524.